Separation Science and Technology
Publication details, including instructions for authors and subscription information:
http://www.informaworld.com/smpp/title~content=t713708471

A Silicon Microseparator based Pervaporation Process for Separation of Ethanol/Water Mixtures using a Polymer Membrane

Sudhir Ramprasad[a]; James D. Palmer[a]
[a] Department of Chemical Engineering, Louisiana Tech University, Ruston, LA, USA

To cite this Article Ramprasad, Sudhir and Palmer, James D.(2007) 'A Silicon Microseparator based Pervaporation Process for Separation of Ethanol/Water Mixtures using a Polymer Membrane', Separation Science and Technology, 42: 11, 2483 — 2499
To link to this Article: DOI: 10.1080/01496390701477170
URL: http://dx.doi.org/10.1080/01496390701477170

Separation Science and Technology, 42: 2483–2499, 2007

ISSN 0149-6395 print/1520-5754 online
DOI: 10.1080/01496390701477170

A Silicon Microseparator based Pervaporation Process for Separation of Ethanol/Water Mixtures using a Polymer Membrane

Sudhir Ramprasad and James D. Palmer
Department of Chemical Engineering, Louisiana Tech University, Ruston, LA, USA

Abstract: The selective removal of water from ethanol through pervaporation was demonstrated in a microchannel device using a commercial membrane. Photolithography and dry etching techniques were employed for fabrication of the microseparator with hydraulic diameters of 30 μm to 80 μm. Experiments conducted at 90°C and 2–3 Torr, with Reynolds Numbers ranging from 8 to 91, resulted in an average water and ethanol permeance of 1.2×10^{-3} and 8×10^{-5} $cm^3/cm^2 \cdot s \cdot cmHg$ respectively. A mass transfer analysis involving Sherwood correlations was used to calculate the theoretical boundary layer resistance. The comparison of overall mass transfer coefficient with the boundary layer coefficients suggests that the membrane was the dominant resistance for this system.

Keywords: Microchemical system, microfluidics, polymer membranes, pervaporation

INTRODUCTION

Microchemical systems are an emerging technology with growing interest for research involved in developing miniaturized chemical processes. Microscale devices are of interest because of their inherent advantages of high surface area to volume ratio, high heat and mass transfer coefficients, large specific surface, shorter residence time, point of use etc. The utilization of

Received 30 September 2006, Accepted 29 May 2007
Address correspondence to James D. Palmer, Department of Chemical Engineering, Louisiana Tech University, Ruston, LA, USA. Tel.: (318)257-2885; E-mail: jpalmer@latech.edu

microchemical systems for several chemical processes has resulted in the process intensification of heat exchangers (1, 2), reactors (3, 4), etc. due to reductions in transport distances. Although these unit operations have been successfully miniaturized, chemical processes will fully benefit only when separation process are integrated in microchemical devices.

Liquid phase separation in a microchemical system by conventional separation techniques has remained a challenge. The conventional separation processes that involve liquid boiling cannot be scaled effectively to a microchemical system due to the surface tension effects that suppress vaporization (5, 6). Microextractors (7, 8) and liquid-liquid contactors (9) are two examples of separation processes that have been successfully miniaturized. Microchemical systems integrated with membrane technology offer tremendous potential as an alternative avenue for separation processes. The commonly involved membranes for gas separation such as palladium membranes have been used in microreactors for hydrogen separation (10, 11) and polymer membranes are reportedly used for product enrichment of ethylene/ethylene oxide mixtures (12, 13) in microchemical systems.

The flow through a microchannel device can be compared to the flow through the bore of a hollow fiber module. Fine hollow fiber membrane modules comprise of fibers with the diameters ranging from 50 to 200 μm (14) similar to that of the microchannel dimensions which range between 10 to 200 μm (6). In particular, the flow in the 120 μm deep channel can be favorably compared to the bore fed hollow fiber membranes with inner diameters of 200–300 μm which have typically been reported in the literature (15–18). A notable similarity between the microchannels and bore fed hollow fibers is in the liquid flow; due to their small hydraulic diameters a laminar regime exists in both the cases. The small hydraulic diameters of both systems result in very high ratios of membrane surface area to fluidic volume. However, the small hydraulic diameters that allow high surface area to volume ratios also result in relatively high pressure drops. An advantage of the system in this study is that conventional flat sheet membranes can be utilized rather than the special fabrication required for a hollow fiber membrane. As such, the microchannel system can complement hollow fiber studies by allowing various membranes types to be screened and tested committing to the fabrication of a hollow fiber membrane.

The synergy of membrane technology and microfluidics has provided a platform for several new applications and research in these areas have a wide array of focus. Lammertink et al. have outlined the scope and prospects of this confluence in their recent review on membranes and microfluidics (19). Researchers have miniaturized diffusion limited conventional membrane processes such as dialysis, pervaporation, and reverse osmosis. To date, only two groups have reported pervaporation studies in microscale devices. Yeung et al. have developed a stainless steel plate membrane microreactor consisting of 35 channels of 300 μm in width, 600 μm in depth, and 2.5 cm in length that selectively separated water by a pervaporation process from Knoevenagel condensation reaction of benzaldehyde and ethyl cyanoacetate

solutions using a hydrophilic ZSM-5 zeolite membrane. They observed that the average permeation rate of pure water through the ZSM-5 membrane was 0.04 kg/m^2 hr at a residence time of 0.13 h, and this rate improved to 0.15 kg/m^2 hr for a longer residence time of 0.8 h. They have reported an increase in 25% conversion in addition to improved product quality by using membrane microreactor (20–22). Eijkel et al. have developed microfluidic channel structures for osmosis and pervaporation using polyimide. Their design consisted of polyimide walls of 4 mm long and 500 nm high arranged in arrays of 16 parallel channels 2–30 μm width. They have reported a seven-fold increase in concentration of KNO_3 solution by dehydrating water using polyimide by pervaporation process (22).

Research involving the pervaporation process in the microscale to study the effects of concentration polarization and process intensification effects in separation performance has not been reported to date. Ethanol/water separation in the microscale pervaporation process delineates an attempt to approach to the prevailing problem of concentration polarization in pervaporation systems. The pervaporation process for separation of highly volatile organics from water has been widely studied for concentration polarization effects and it has been reported that the transport resistance through the boundary layer is dominating (23–34). However, there are limited reports in the literature on concentration polarization with ethanol/water dehydration. It has been reported by Neel (35) that during the separation of ethanol/water azeotrope using a polyvinylalcohol-based GFT membrane, the boundary layer is significant only when the feed water concentration is less than 1% by weight. Many researchers have developed techniques to minimize the effect of concentration polarization by focusing their efforts in developing novel membrane modules such as vibrating module (36) or other techniques such as using turbulent promoters, pulsing feed flow over the membrane, etc. (37). The ultimate goal of these researchers was to increase the mass transfer coefficient in the boundary layer. In a conventional pervaporation process sensitive to concentration polarization, the boundary layer thickness is a function of the flow velocity. In the present study, a silicon microseparator was developed with the largest hydraulic diameter of 80 μm. This hydraulic diameter is smaller than the boundary layer thickness typically present in the conventional pervaporation systems for laminar flow. Incorporating microfluidic channels for fluid flow in the membrane module should therefore provide a potential solution for reducing the boundary layer resistance in systems that exhibit concentration polarization effects.

EXPERIMENTAL

Microseparator Fabrication

The microseparator consisted of an inlet and outlet via with the microchannels placed between the inlet and the outlet as shown in the picture of the fabricated

Figure 1. Top view of silicon microseparator.

microseparator in Fig. 1. The microseparator was fabricated by conventional photolithography and deep reactive ion etching (DRIE) on a ⟨100⟩ orientation, single side polished, silicon wafer of ~500 μm thickness and 4 inches in diameter. An emulsion mask of the design was generated using a high-resolution printer and transferred to a chrome mask to facilitate alignment. A positive photoresist (Shipley 1813) was spin-coated on the cleaned polished face of the silicon wafer. This photoresist was used on the front side of the wafer to transfer patterns of the microchannels. UV light (g-line, 7 w/cm^2) was exposed through a chromemask using a mask aligner (EVG) to transfer the microseparator pattern on to the photoresist. The silicon microchannels were etched by DRIE, using Inductive Coupled Plasma (Alcatel A601 E). ICP etching facilitates in obtaining perpendicular walls with high aspect ratio as shown in the SEM picture in Fig. 2. After the fabrication of the microchannels on the front side, the back side of the wafer was spin-coated with a thick photoresist (AZ 9260) to transfer the inlet and outlet via patterns. DRIE was also performed to etch the inlet and outlet vias. The fabricated microseparator consisted of 99 microchannels 60 μm wide of 3 cm length. Microseparator depths of 22, 47, and 120 μm were fabricated for testing.

Description of Membrane Module/in-situ Heat Exchanger

The membrane module/in-situ heat exchanger was machined from an aluminum block (0.5 inch thick) and the schematic is shown in Fig. 3. This module consisted of a top plate and a bottom plate (each 2.5 × 3.65 inches)

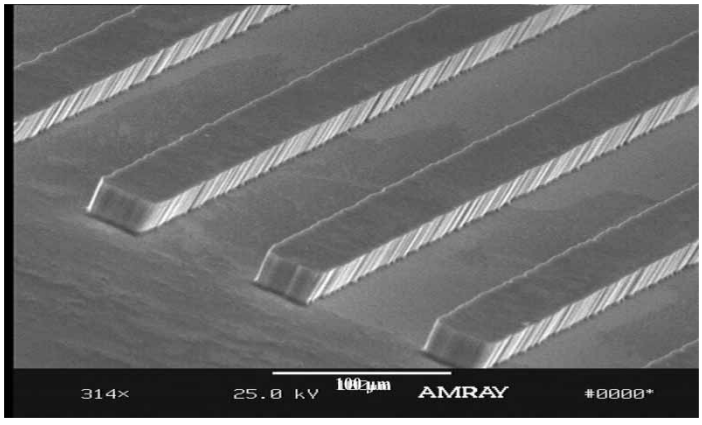

Figure 2. SEM image of microchannels, fluid is directed between raised columns.

and the bottom plate consisted of inlet and outlet ports for fluidic connections. A circulator (Polyscience, Model 9510) was used to circulate 100% ethylene glycol maintained at a temperature higher than the target operating temperature. An external RTD (Resistance Temperature Detector) temperature probe (Weed Instruments) connected to the circulator facilitated in establishing an efficient contact for temperature measurement on the membrane module. The temperature in the membrane module was acquired by a computer using the commercial software Labworldsoft v 4.5.

Pervaporation

Pervaporation experiments were performed with the apparatus schematically shown in Fig. 4. Pervaporation of ethanol/water mixture through the

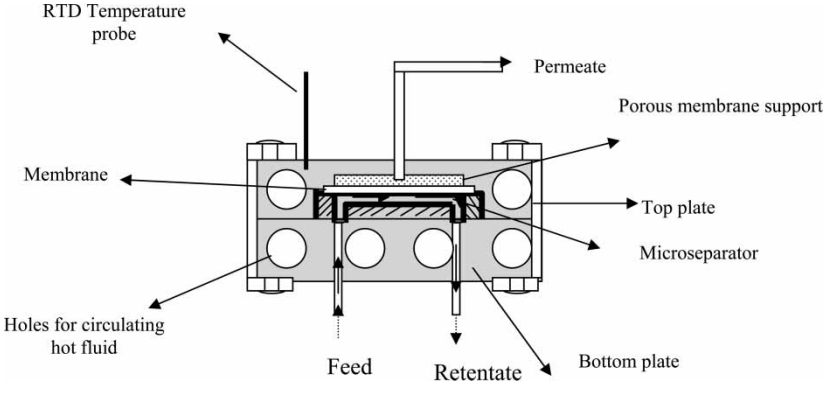

Figure 3. Schematic of the membrane module/in-situ heat exchanger.

membrane was carried out using a microseparator housed inside an aluminum membrane module as described earlier. The effective permeation area of the Sulzer chemtech PERVAP 2216 membrane was 1.78 cm^2. The feed binary mixture of 90 wt% ethanol was prepared using reagent grade ethanol (Sigma Aldrich) in deionized water. The feed tank used was a 50 ml glass beaker. The feed ethanol solution (~33 ml as initial volume) was re-circulated through the membrane module back to the feed tank. The feed tank was placed on an analytical balance (Ohaus explorer) and the mass changes that occurred in the feed tank as a result of selective removal of water from the membrane during pervaporation were continuously acquired by a computer for every 10 seconds. A Masterflex feed pump was used to circulate the feed solution through the microseparator. The feed flow rates used in the experiments were in the range of 1–50 ml/min corresponding to velocities of 0.12–1.30 cm/s. All experiments were performed at a constant temperature of 90°C. A vacuum pump (Welch Chemstar 1376 N) provided the required vacuum, and a vacuum pressure of 2–3 Torr was maintained for all the experiments. An analog pressure gauge (Supco) was used to measure the vacuum pressure. A vacuum trap (Chemglass) immersed in liquid nitrogen housed in a dewar flask was used to condense the permeate vapors.

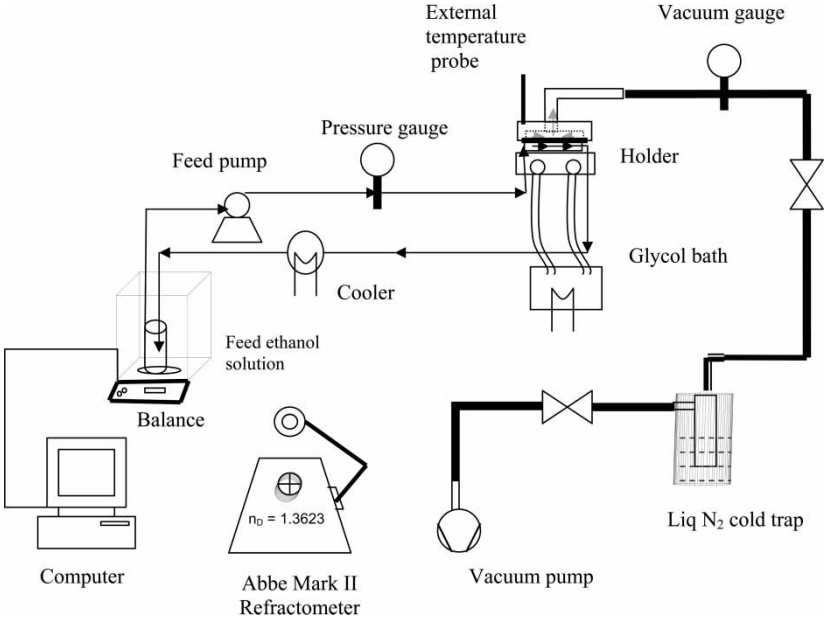

Figure 4. Schematic of the pervaporation experimental set-up for the silicon microseparator.

A high precision Abbe Mark II refractometer (Reichert Inc) was used to analyze the ethanol concentration in the feed tank. All refractive index measurements were made at a constant temperature of 20°C. A section of the retentate line from the experimental set-up was immersed in this water bath in order to maintain the temperature of the ethanol solution in the feed tank at room temperature. A temperature probe (Type K thermocouple) from a digital multimeter (Extech, Model 382860) was placed inside the feed tank to monitor the temperature of the feed solution during the experiment. This temperature data was acquired by a computer for every 30 seconds through out the duration of the pervaporation experiment.

The small mass permeated through the membrane precluded effective capture of the permeate for analysis of the membrane performance. A differential mass balance of the system, using the retentate mass balance data acquired continuously and the retentate ethanol concentration measured periodically as inputs, was used to determine the flux and selectivity of the membrane.

Theory

To predict the impact that the channel dimension and velocity would have on the overall mass transfer coefficient of the system, the commonly used resistance-in-series model was employed (32). Three resistances are noted during transport in membrane separation:

a) Mass transfer from the feed bulk to the feed membrane surface
b) Diffusion through the membrane
c) Desorption at the membrane permeate interface

Assuming the desorption at the membrane permeate interface is negligible; the overall mass transfer resistance is the sum of the membrane resistance and the boundary layer resistance.

$$R_{ov} = R_{bl} + R_m \tag{1}$$

R_{ov} = Overall resistance
R_{bl} = Boundary layer resistance
R_m = Membrane resistance

The mass transfer coefficients are reciprocal of the respective resistances.

$$\frac{1}{k_{ov,i}} = \frac{1}{k_{bl,i}} + \frac{1}{k_{m,i}} \tag{2}$$

The flux through the membrane can be given by the following equation.

$$J_i = k_{ov,i} C_{b,i} \tag{3}$$

Sherwood Correlations

It is important to choose the appropriate semi-empirical Sherwood correlation in order to accurately predict the role of boundary layer resistance. Reviewing the literature, it was observed that for laminar flow the following correlations have been reported (15, 38–43). In Eqs. (4–6) the values of coefficients a, b, c reported by different authors are shown in Table 1.

$$Sh = C + a\left(\mathrm{Re}\ \delta_c \left(\frac{D_h}{L}\right)\right)^b \tag{4–6}$$

Eqs. (4) and (5) are applicable in the developing region of the channel. Eq. (6) is applicable for both the developing and fully developed region. The short microchannel length and large range of flow velocities tested resulted in situations that varied between completely developed profiles for the majority of the channel to developing profiles continuing at the exit of the channel. As noted in the introduction, the flow regime and channel dimensions of the microchannels are similar to studies reported in the literature on hollow fiber membrane modules where the liquid is fed through the capillary bore and the permeate is removed in the outside shell. The majority of these studies utilize Eq. (4) to calculate the Sherwood number. However, Eq. (6) was utilized in this article to allow both the developing and fully developed regions to be modeled. The Sherwood number used to calculate the boundary layers and mass transfer resistances below was determined using Eq. (6) at every 0.1 cm increment of the microchannel and taking an average over the entire 3 cm length.

$$\delta_i = \frac{D_h}{Sh} \tag{7}$$

δ_i = Boundary layer thickness.

Table 1. Coefficients for Sherwood correlations

	Coefficients in the Sherwood correlations			
Eq.	Ref.	C	a	b
(4)	(32)	—	1.62	0.33
(5)	(33)	—	1.85	0.33
(6)	(34, 35)	3.66	1.61	0.33

The Reynolds number, Re, is the dimensionless parameter that describes the feed flow conditions;

$$\mathrm{Re} = \frac{D_h \mathrm{v} \rho}{\mu} \tag{8}$$

The Schmidt number, Sc, relates the diffusivity of momentum and the diffusivity of mass in the feed,

$$Sc = \frac{\eta}{D_i} \tag{9}$$

η = Kinematic viscosity of ethanol solution at 90°C.
The boundary layer mass transfer coefficient can be calculated by simple manipulation of Eq. (7).

$$k_{bl} = \frac{D_i Sh}{D_h} \tag{10}$$

$\mathrm{D_i}$ = Diffusion coefficient of water in ethanol at 90°C (44)
$D_h = 2wd/w + d$ = Hydraulic diameter

w = Width of the microchannel
d = Depth of the microchannel
L = Length of the microchannel
v = Velocity of the fluid in the microchannel
ρ = Density of ethanol solution at 90°C
μ = Viscosity of ethanol solution at 90°C

From the above correlations, the dependence of velocity on boundary layer thickness can be described by Eq. (11). Eqs. (12) and (13) depict the dependence of hydraulic diameter on boundary layer thickness for situations involving constant volumetric flow-rate, constant Reynolds Number, and constant velocity with Table 2 providing the constants C1 and C2 for these relationships.

$$\frac{\delta_1}{\delta_2} = \left(\frac{\nu_2}{\nu_1}\right)^{\frac{1}{3}} \quad \text{Constant hydraulic diameter} \tag{11}$$

$$\frac{\delta_1}{\delta_2} = \left(\frac{D_{h1}}{D_{h2}}\right)^{C_1} \tag{12}$$

$$\frac{dP_1}{dP_2} = \left(\frac{D_{h1}}{D_{h2}}\right)^{C_2} \tag{13}$$

dP = Pressure drop

Table 2. Exponents relating hydraulic diameter to boundary layer thickness and pressure drop

Eq.	C	Constant volumetric flow	Constant Reynolds number	Constant velocity
(12)	C_1	1	2/3	1/3
(13)	C_2	4	3	2

As evident from the above correlations, the boundary layer thickness has a higher dependence with hydraulic diameter than velocity if the Reynolds Number is maintained as a constant, however the pressure required rises dramatically as the hydraulic diameter is reduced. The ten-fold increase in velocity tested in each microchannel resulted in a predicted decrease of 22%, 36%, and 40% in boundary layer thickness for the 22, 47, and 120 μm deep microchannels respectively. The 5.5 fold decrease in depth from 120 to 22 μm resulted in a predicted decrease of 53% in boundary layer thickness at the lowest velocity tested but only a 39% decrease at the highest velocity tested. Therefore, from the predictions of the mass transfer correlations it appears that reducing channel dimensions to reduce boundary layer thickness will be most advantageous when low velocities are desired or required for a given application.

RESULTS AND DISCUSSION

The separation of water from ethanol was used to demonstrate the performance of the microfluidic device. The effect of operating parameters on separation performance will be discussed. The resistance-in-series model was used to determine the rate-limiting sequence in the series of mass transfer steps involved during the transport of the solute from the bulk and through the boundary layer and membrane as the permeate. The transport resistance calculations for the boundary layer and the overall resistance will be reported.

To calculate the overall mass transfer coefficient for water transport from the experimental values, a graph of water flux vs. feed water concentration was plotted. The slope of the linear regression from this plot directly provided the overall mass transfer coefficient. In all experiments a high order of linearity ($r^2 > 0.99$) was observed. This method was used to calculate the overall mass transfer coefficient in all the experiments.

The model developed by Wijmans and Baker (45) for predicting the experimental data in terms of permeate flux normalized with the driving force was used to analyze the performance of the membrane separator. The permeance calculations was based on the transport equation from the

solution-diffusion model

$$J_i = Q_i(x_i \gamma_i p_i^s - y_i p_i) \tag{14}$$

J_i = Permeate flux of component i
Q_i = Permeance of component i
x_i = Liquid mole fraction of component i in the feed
γ_i = Activity coefficient of component i in the feed
p_i^s= Saturation pressure of the pure component i at the operating temperature
y_i = Vapor mole fraction of component i
p_i = Permeate pressure

Using the relevant data (46) for ethanol-water system, the saturation pressure p_i^s was calculated using Antoine's (44) equation and the activity coefficients were calculated using Wilson's equation (44).

The influence of operating temperature on permeance for 9, 7, and 5 w/w % water concentration in the feed and at a feed flow rate of 5 ml/min in the 22 μm deep channels was evaluated. Operating temperatures tested included 70, 80, and 90°C. The water permeance remained constant or increased slightly as the feed water concentration was increased (Fig. 5), but the water permeance did increase as the operating temperature was increased. T.S. Chung (47) reported a similar trend using a Sulzer Chemtech PERVAP 2201 membrane for the dehydration of isopropanol and butanol isomers. These authors suggest that water permeance of membranes with high cross-linking and hydrophobicity will be more sensitive to changes in operating temperature than changes in water feed concentration.

The primary objective of the study was to determine if smaller microchannel dimensions facilitated shorter diffusion distances resulting in a favorable impact on the overall mass transfer coefficient of the chosen system. The sensitivity of flow-rate to the overall mass transfer coefficient was also examined in this study. The water and ethanol permeance were plotted against Reynolds number and hydraulic diameter. Figures 6 and 7 depict the behavior of ethanol and water permeance at an intermediate feed water concentration of 6 wt%. As described earlier, the experiments were conducted with an initial feed tank water concentration of 10 wt%. The feed tank water concentration decreased to approximately 3 wt% over the course of the experiment. As discussed earlier, the water and ethanol permeance did not exhibit a significant change within the range of concentrations tested. As such, an intermediate feed water concentration of 6 wt% was chosen to demonstrate behavior when the Reynolds number and hydraulic diameter was varied. The objective of comparing changes in Reynolds Number and the hydraulic diameter was to determine if either impacted separation performance. If the mass transfer coefficient is the dominant resistance of the membrane system, the reduction in channel depth from 120 μm to 22 μm as predicted by the Sherwood correlation developed in the previous section should result in slightly over two-fold

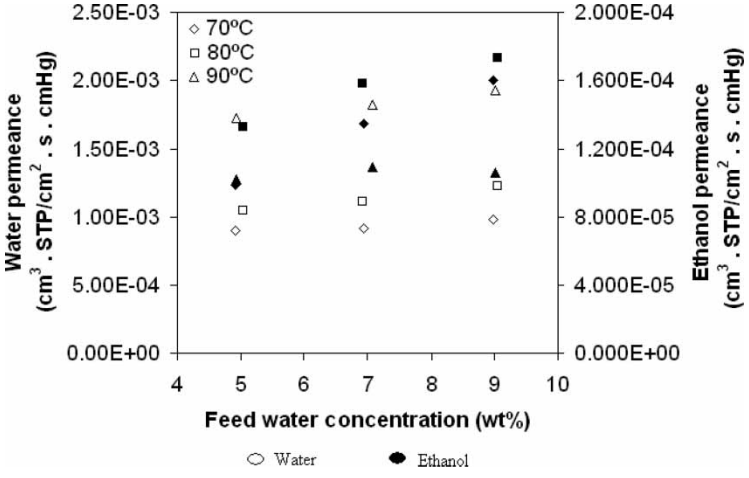

Figure 5. Water and Ethanol permeance vs. feed water concentration at different temperatures.

increase in mass transfer coefficient. The graphs exhibit an average water permeance of 1.2×10^{-3} and ethanol permeance of 8×10^{-5} $cm^3/cm^2 \cdot s \cdot cmHg$. However, there the data appears dispersed with little correlation to Reynolds number or hydraulic diameter.

To understand the reasons for the dispersion in the data, the experimental overall mass transfer resistance was graphed with each predicted boundary layer resistance versus Reynolds Number. Figure 8 depicts a three order of

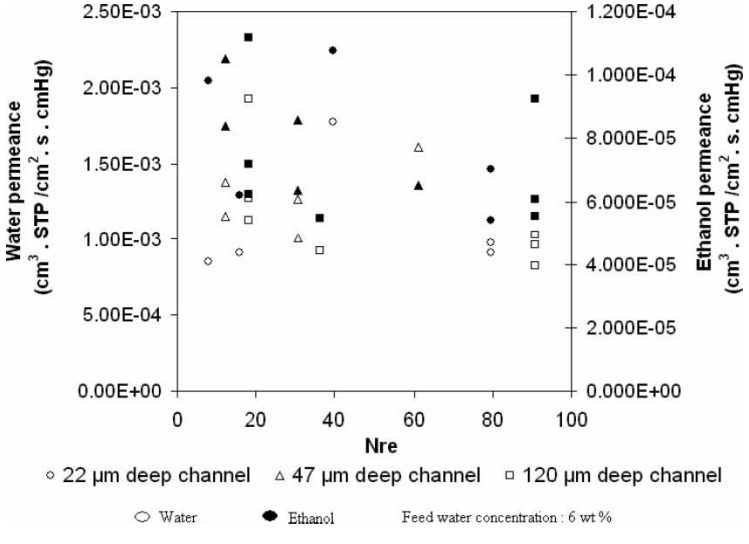

Figure 6. Effect of water and ethanol permeance at varying Reynolds number.

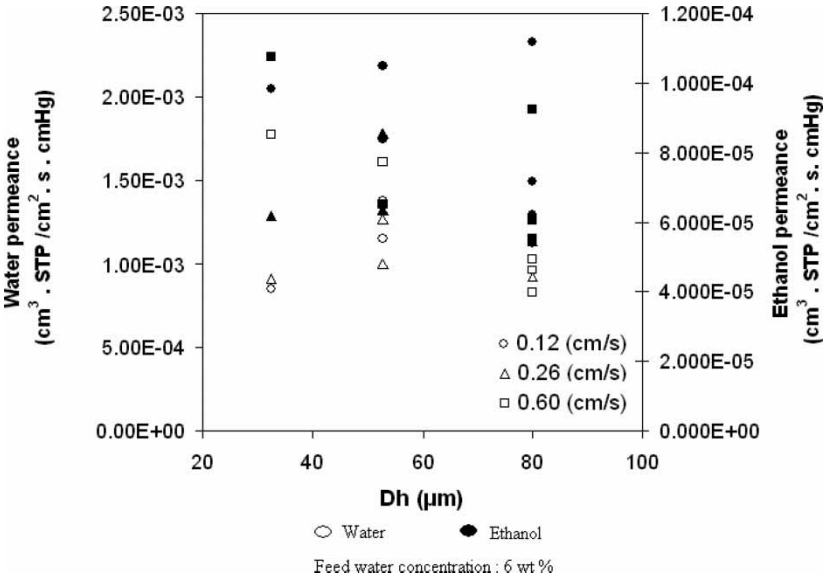

Figure 7. Effect of water and ethanol permeance at different hydraulic diameter.

magnitude difference in the observed and predicted boundary layer resistances in the system. Indeed, the y-axis of the graph is plotted on a logarithmic scale to emphasize the difference in the resistances evaluated. Clearly the ethanol dehydration membrane chosen, at the conditions operated, was the dominant

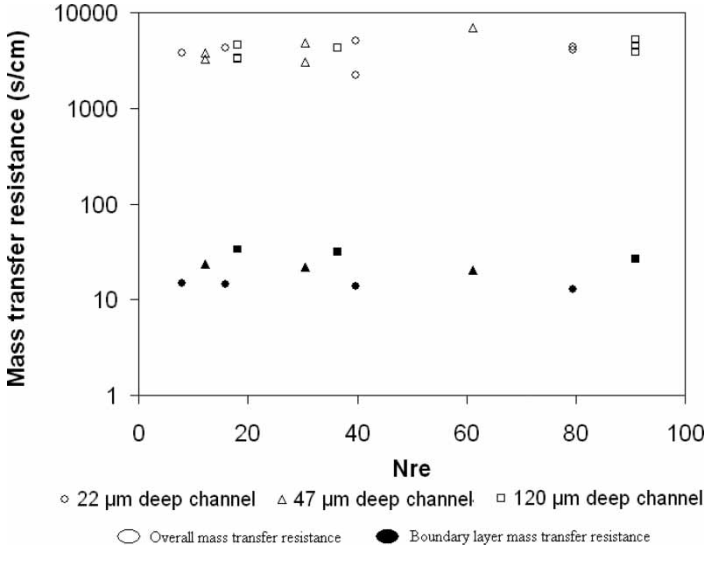

Figure 8. Effect of mass transfer resistance at varying Reynolds number.

resistance and therefore did not benefit significantly from the reduction in hydraulic diameter. Systems that have demonstrated significant boundary layer resistances in the literature would benefit the greatest from the reduction in hydraulic diameter. For example, trichloroethylene (TCE) has a reported diffusivity that is higher in PDMS than an aqueous environment (36), and is a classic example in the literature of a pervaporation system that exhibits significant boundary layer resistance. TCE removal from water and similar systems would be appropriate choices for future studies in microchemical separation, especially for applications requiring a laminar or low flow velocity.

CONCLUSIONS

This work reports the performance of a microchannel separator for ethanol dehydration.

Hydraulic diameters tested ranged from 30 to 80 μm. The flow rates tested in this set-up corresponded to Reynolds number within the range of 8 to 91. In these experiments an operating temperature of 90°C and a low vacuum pressure of 2–3 Torr favored high separation performance. In-depth mass transfer analysis was developed by adapting resistance-in-series model and Sherwood correlations. The model predicted a significant reduction in boundary layer resistance should be obtained by reducing the hydraulic diameter, and within the laminar regime the reduction in hydraulic diameter has a stronger influence on mass transfer than velocity. The experimental results did not exhibit the higher overall mass transfer coefficient predicted because the contribution of resistance by the boundary layer was three orders of magnitude lower than that observed for the entire system and therefore the membrane was the dominant resistance. Recommendations for future studies should be focused on systems that have demonstrated high boundary layer resistance in the literature, such as the removal of TCE from water, if the full benefits of the reduction in the hydraulic diameter are to be realized.

ACKNOWLEDGEMENTS

We gratefully acknowledge the support of NSF grant # 0407097, Dr. Hisham Hegab PI.

REFERENCES

1. Schubert, K., Bier, W., Brandner, J., Fichtner, M., Franz, C., and Linder, G. (1998) Realization and testing of microstructure reactors, micro heat exchangers and

micromixers for industrial applications in chemical engineering. In Process Miniaturization: 2nd International Conference on Microreaction Technology, IMRET 2, AIChE New Orleans, USA; Ehrfeld, W., Rinard, I.H. and Wegeng, R.S. (eds.); Topical Conference Preprints, 88.
2. Ehrfeld, W., Hessel, V., and Haverkamp, V. (1999) *Microreactors in Ullmann's Encyclopedia of Industrial Chemistry*, 6th Edn; Wiley-VCH: Weinheim.
3. Mazanec, T., Perry, S., Tonkovich, L., and Wang, Y. (2004) Microchannel gas-to-liquids conversion-thinking big by thinking small. *Studies in Surface Science and Catalysis*, 169–174.
4. Lowe, H., Hessel, V., and Mueller, A. (2002) Microreactors. Prospects already achieved and possible misuse. *Pure Appl. Chem.*, 74 (12): 2271–2276a.
5. Zhang, L., Wang, E.N., Goodson, K.E., and Kenny, T.W. (2005) Phase change phenomena in silicon microchannels. *Intl. J. Heat and Mass Transfer.*, 48: 1572–1582.
6. Kandilkar, S.G. (2004) Heat transfer mechanisms during flow boiling in microchannels. *J. Heat Transfer.*, 126: 8–16.
7. Aracil, C.J. and Quero, J.M. (2005) Microextractor controlled, Proceedings of SPIE-The International Society for Optical Engineering. Smart Sensors, Actuators, and MEMS II; 5836: 617–624.
8. Wang, X., Saridara, C., and Mitra, S. (2005) Microfluidic supported liquid membrane extraction. *Anal. Chim. Acta*, 543: 92–98.
9. Martin, P.M., Matson, D.W., and Bennet, W.D. (1999) Microfabrication methods for microchannel reactors and separation systems. *Chem. Engg. Comm.*, 173: 245–254.
10. Zheng, A., Jones, F., and Fang, J. Dehydrogenation of cyclohexane to benzene in a membrane microreactor, Annual Conference on Microreaction Technology, AIChE, Spring National Meeting, Atlanta, GA, (March 5–9, 2000).
11. Franz, A.J., Jensen, K.F., and Schmidt, M.A. (1999) Palladium Membrane micro reactors, Proceedings of the 3rd International Conference on Micro Reaction Technology, 267–276.
12. Schiewe, B., Vuin, A., Gunther, N., Gebauer, K., Richter, Th., and Wegner, G. (1999) Polymer membranes for product enrichment in microreactor technology. Proceedings of the 3rd International Conference on Micro Reaction Technology; 550–555.
13. Schiewe, B., Vuin, A., Gunther, N., Gebauer, K., Richter, Th., and Wegner, G. (2001) Membrane-based gas separation of ethylene/ethylene oxide mixtures for product enrichment in microreactor technology. *Chemphyschem*, 2: 211–218.
14. Baker, R.W. (2000) *Membrane Technology and Applications*; McGraw –Hill: New York, 132.
15. Crowder, M.L. and Gooding, C.H. (1997) Spiral wound-hollow fiber membrane modules- a new approach to higher mass transfer efficiency. *J. Membr. Sci.*, 137: 17–29.
16. Sirkar, K.K. and Prasad, R. (1988) Dispersion-free solvent extraction with microporous hollow-fiber modules. *AICHE. J*, 34 (2): 177–187.
17. Asimakopoulou, A.G. and Karabelas, A.J. (2006) A study of mass transfer in hollow-fiber membrane contactors-the effect of fiber packing fraction. *J. Membr. Sci.*, 282: 430–441.
18. Abou-Nemeh, I., Das, A., Saraf, A., and Sirkar, K.K. (1998) A composite hollow fiber membrane-based pervaporation process for separation of VOCs from aqueous surfactant solutions. *J. Membr. Sci.*, 158: 187–209.

19. Jong, J.de., Lammertink, R.G.H., and Wessling, M. (2006) Membranes and microfluidics: a review. *Lab Chip*, 6: 1125–1139.
20. Lai, S.M., Ng, C.P., Aranda, R.M., and Yeung, K.L. (2003) Knoevenagel condensation reaction in zeolite membrane microreactor. *Microporous and Mesoporous*, 66: 239–252.
21. Zhang, X., Lai, S.M., Aranda, R.M., and Yeung, K.L. (2004) An investigation of knoevenagel condensation reaction in microreactors using a new zeolite catalyst. *Appl. Catal. A*, 261: 109–118.
22. Eijkel, J.C.T., Bomer, J.G., and Van Den Berg, A. (2005) Osmosis and pervaporation in polyimide submicron microfluidic channel structures. *Appl. Phys. Lett.*, 87 (n11): 103–114.
23. Psaue, R., Aptel, Ph., Aurelle, Y., Mora, J.C., and Bersillon, J.L. (1988) Pervaporation: importance of concentration polarization in the extraction of trace organics from water. *J. Membr. Sci.*, 36: 373–384.
24. Raghunath, B. and Hwang, S.-T. (1992) General treatment of liquid-phase boundary layer resistance in the pervaporation of dilute aqueous organics through tubular membranes. *J. Membr. Sci.*, 75: 29–46.
25. Raghunath, B. and Hwang, S.-T. (1992) Effect of boundary layer mass transfer resistance in the pervaporation of dilute organics. *J. Membr. Sci.*, 75: 147–161.
26. Feng, X. and Huang, R.Y.M. (1994) Concentration polarization in pervaporation separation processes. *J. Membr. Sci.*, 92: 201–208.
27. Rautenbach, R. and Helmus, F.P. (1994) Some consideration on mass-transfer resistances in solution-diffusion-type membrane processes. *J. Membr. Sci.*, 87: 171–181.
28. Dotremont, C., Van den Ende, S., Vandommele, H., and Vandecasteele, C. (1994) Concentration polarization and other boundary layer effects in the pervaporation of chlorinated hydrocarbons. *Desalination*, 95: 91–113.
29. Wijmans, J.G., Athayde, A.L., Daniels, R., Ly, J.H., Kamaruddin, H.D., and Pinnau, I. (1996) The role of boundary layers in the removal of volatile organic compounds from water by pervaporation. *J. Membr. Sci.*, 109: 135.
30. Jiang, J-S., Vane, L.M., and Sikdar, S.K. (1997) Recovery of VOCs from surfactant solutions by pervaporation. *J. Membr. Sci.*, 136: 233–247.
31. Bhattacharya, S. and Hwang, S.-T. (1997) Concentration polarization, separation factor, and Peclet number in membrane processes. *J. Membr. Sci.*, 132: 73–90.
32. Baker, R.W., Wijmans, J.G., Athayde, A.L., Daniels, R., Ly, J.H., and Le, M. (1997) The effect of concentration polarization on the separation of volatile organic compounds from water by pervaporation. *J. Membr. Sci.*, 137: 159–172.
33. Jou, J., Yoshida, W., and Cohen, Y. (1999) A novel ceramic-supported polymer membrane for pervaporation of dilute volatile organic compounds. *J. Membr. Sci.*, 162: 269–284.
34. Liang, L., Dickson, J.M., Jiang, J., and Brook, M.A. (2004) Effect of low flow rate on pervaporation of 1,2-dichloroethane with novel polydimethylsiloxane composite membranes. *J. Membr. Sci.*, 231: 71–79.
35. Neel, J. (1995) Pervaporation. In *Membrane Separations Technology Principles and Applications*; Noble, R.D. and Stern, S.A. (eds.); Elsevier Science Publishers B.V: Amsterdam, 186.
36. Vane, L.M., Alvarez, F.R., and Grioux, E.L. (1999) Reduction of concentration polarization in pervaporation using vibrating membrane module. *J. Membr. Sci.*, 153: 233–241.
37. Matthiasson, E. and Sivik, B. (1980) Concentration polarization and fouling. *Desalination*, 35: 59–103.

38. Karlsson, H.O.E. and Tragardh, G. (1993) Aroma compound recovery with pervaporation–feed flow effects. *J. Membr. Sci.*, 81: 163–171.
39. Porter, M. (1972) Concentration polarization with membrane ultra filtration. *Ind. Eng. Chem. Prod. Res. Develop.*, 11 (3): 234–248.
40. Gekas, V. and Hallstrom, B. (1987) Mass transfer in the membrane concentration polarization layer under turbulent cross flow I. Critical literature review and adaptation of existing Sherwood correlations to membrane operations. *J. Membr. Sci.*, 30: 153–170.
41. Huang, R.Y.M. (1991) *Pervaporation Membrane Separation Process*; Elsevier Science Publishers B.V: Amsterdam, 193.
42. Rautenbach, R. and Helmus, F.P. (1994) Some consideration on mass-transfer resistances in solution-diffusion-type membrane processes. *J. Membr. Sci.*, 87: 171–181.
43. Crowder, R.O. and Cussler, E.L. (1998) Mass transfer resistances in hollow fiber pervaporation. *J. Membr. Sci.*, 145: 173–184.
44. Reid, R.C., Prausnitz, J.M., and Poling, B.E. (1987) *The Properties of Gases & Liquids*, 4th Edn.; McGraw-Hill: New York, 616.
45. Wijmans, J.G. and Baker, R.W. (1993) A simple predictive treatment of the permeation process in pervaporation. *J. Membr. Sci.*, 79: 101–113.
46. Gmehling, J. and Onken, U. (1991) *Vapor-liquid Equilibrium Data Collection: Aqueous-Organic Systems; DECHEMA Chemistry Data Series Vol. I, Part I*, 2nd edn; DECHEMA Deutsche Gesellschaft fur Chemisches Apparatewesen: 171.
47. Qiao, X., Chung, T.-S., Guo, W.F., Matsuura, T., and Teoh, M.M. (2005) Dehydration of isopropanol and its comparison with dehydration of butanol isomers from thermodynamic and molecular aspects. *J. Membr. Sci.*, 252: 37–49.